Comput Mech (2009) 44:377–393
DOI 10.1007/s00466-009-0376-5

ORIGINAL PAPER

A C^k continuous generalized finite element formulation applied to laminated Kirchhoff plate model

Clovis Sperb de Barcellos · Paulo de Tarso R. Mendonça · Carlos A. Duarte

Received: 5 December 2008 / Accepted: 30 January 2009 / Published online: 10 March 2009
© Springer-Verlag 2009

Abstract A generalized finite element method based on a partition of unity (POU) with smooth approximation functions is investigated in this paper for modeling laminated plates under Kirchhoff hypothesis. The shape functions are built from the product of a Shepard POU and enrichment functions. The Shepard functions have a smoothness degree directly related to the weight functions adopted for their evaluation. The weight functions at a point are built as products of C^∞ edge functions of the distance of such a point to each of the cloud boundaries. Different edge functions are investigated to generate C^k functions. The POU together with polynomial global enrichment functions build the approximation subspace. The formulation implemented in this paper is aimed at the general case of laminated plates composed of anisotropic layers. A detailed convergence analysis is presented and the integrability of these functions is also discussed.

Keywords Generalized finite element method · Partition of unity method · Kirchhoff plate FEM · C^k continuous approximation functions

C. S. de Barcellos (✉) · P. de Tarso R. Mendonça (✉)
Mechanical Engineering Department, Federal University of Santa Catarina, 88040-900 Florianópolis, SC, Brazil
e-mail: clovis@grante.ufsc.br

P. de Tarso R. Mendonça
e-mail: mendonca@grante.ufsc.br

C. A. Duarte
2122 Newmark Civil Engineering Laboratory,
University of Illinois at Urbana-Champaign, 205 North Mathews Ave., Urbana, IL 62801-2352, USA
e-mail: caduarte@uiuc.edu

1 Introduction

In the last decade a number of meshless procedures have been proposed in the FEM community. These include, among several others, the smoothed particle hydrodynamics method [27], the diffuse element method [37], wavelet Galerkin method [1], the element free Galerkin method (EFGM) [12], reproducing Kernel particle method (RKPM) [32], the meshless local Petrov-Galerkin method [2], the natural element method [46], partition of unity method [3], and the *hp*-clouds methods e.g. [20,21]. The latter has the further appeal of naturally introducing a procedure for performing *p*-adaptivity, in a very flexible way, avoiding the construction of functions by sophisticated hierarchical techniques. The advantages of these procedures are, however, balanced by increased computational cost since a mesh is still needed for integration purposes and, at each integration point, the partition of unity (POU) must be independently computed since the covering of each point is arbitrary.

The *hp*-clouds approximations have been proved to be more efficient than others like the EFGM [21,22], and for this reason they were used in [26,36]. But all these meshless methods present some disadvantages regarding the imposition of boundary conditions and high computational costs. In order to ameliorate the cost of numerical integration and the implementation difficulties of mesh free methods, Oden et al. [38], proposed that, instead of using circles or rectangles for defining the clouds around each node, it would be more convenient to use linear finite element meshes. Here the clouds associated with a node "i" is built by the union of the "elements" connected to this node. This concept greatly reduces the number of floating point operations, since the POU is known beforehand and allows standard integration routines for integrating the nodal matrices. This new scheme led to a generalized finite element method (GFEM).

Independently, Babuška and coworkers proposed essentially the same procedure, initially named as special finite element method [34], and later as the partition of unity finite element method [4]. A similar philosophy is inserted in the works of Belytschko and Black [10], and Moës et al. [35] for discontinuous solutions and is called extended finite element method (XFEM). The *p*-enrichment, as in other meshfree methods like *hp*-clouds, are performed nodally, which suggests an adaptive scheme to provide automatic control of approximation errors. Several contributions have been proposed, among them are the works of Strouboulis et al. [45], Babuška et al. [4], Belytschko et al. [11], Liu et al. [32], and Barros et al. [5]. In such procedures, the solution improvement is reached by only performing nodal enrichment without excessively increasing the computational effort even in presence of stress concentration [19], thus reducing the possible need to perform a mesh refinement in this type of problems.

The usual GFEM scheme leads only to C^0 approximation functions. On the other hand, there are several models, like the Kirchhoff plate, which require solutions to be at least C^1 continuous. This requirement has led to several finite element formulations which release such a need under the cost of lower accuracy and/or consistency. Many other formulations are based on mixed or hybrid variational principles for coping with such difficulties like, e.g. [7]. In many circumstances, the Mindlin's and Reissner's models, which requires only C^0 continuity, have been dominant over the last decades, e.g. [15]. In recent years, some meshless methods have been proposed for solving Kirchhoff plate and shell models [8,9,16,30,31,33,43]. Again, another approach to reduce the numerical integration costs and boundary conditions difficulties of the meshless methods was proposed by Edwards [24,25], in which a finite element mesh is used to build arbitrarily smooth approximation functions which have the same support of corresponding global finite element Lagrangean shape functions on the same mesh. This scheme has an important restriction for requiring the clouds to be convex, which is not always possible to guarantee. Aiming at removing this limitation, Duarte et al. [18] used the so-called boolean R-function of Shapiro [41]. Latter, Barros et al. [6] discusses this procedure for linear elasticity problems. The arbitrary continuity is based on the type of selected edge functions and on the value of a parameter of a boolean function.

In addition, the higher degree of regularity has the advantage of enhancing the definition of error measures as is also pointed out by [11], for the case of the reproducing kernel particle method (RKPM), and also allows strong residual evaluation.

Presently, the authors make use of an extension of the Edwards' approach, utilized by Duarte [18], for convex and non-convex supports with the aid of the so-called *R*-functions [40,41], on GFEM with C^k approximating functions, in triangular unstructured meshes. These sets of approximation functions are applied for solving some Kirchhoff plate problems. The influence of the type of integration rules, Gaussian or triangular rules, is analyzed. Several types of cloud edge functions are implemented and tested.

The remainder of this paper is outlined as follows: Sect. 2 summarizes the partition of unity concepts; Sect. 3 presents the *hp*-cloud partition of unity functions and their enrichment; Sect. 4 develops the construction of weighting functions based on several cloud edge functions in order to achieve C^∞ and C^k continuity on the approximation functions; Sect. 5 presents a summary of the laminated Kirchhoff plate model and Sect. 6 presents results of the proposed formulation in order to test its behavior under several conditions.

2 Partition of unity and approximation functions

Here, the basic idea is to employ weight functions which are zero at the clouds boundaries, together with its first (or higher) normal derivative in order to lead to a C^1 (or higher continuity) partition of unity as it is performed in the *hp*-clouds method. Aiming to summarize such procedure, let us consider a conventional triangular finite element mesh, $\{\mathcal{K}_e\}_{e=1}^{\mathrm{NE}}$ (NE being the number of elements $\mathcal{K}_e$) defined by N nodes, $\{\mathbf{x}_\alpha\}_{\alpha=1}^{N}$, in an open bounded domain $\Omega \subset \mathcal{R}^2(\mathbf{x})$. To each of these nodes, one denotes the interior of the union of the finite elements sharing it as *cloud*, ω_α, $\alpha = 1, \ldots, N$, as is usual in the GFEM. Over each cloud, C^k appropriate weight functions are evaluated and used in the Shepard's moving least square method [42] scheme for generating a partition of unity.

Let an open bounded domain $\Omega \subset \mathcal{R}^2(\mathbf{x})$, here defined as the plate mid-surface, and $\Im_N$ be an open covering of this domain made of the set of N clouds ω_α, associated with nodes $\mathbf{x}_\alpha$. In other words, the closure $\overline{\Omega}$ of the domain is contained in the union of the clouds closures $\overline{\omega}_\alpha$:

$$\overline{\Omega} \subset \bigcup_{\alpha=1}^{N} \overline{\omega}_\alpha \tag{1}$$

One denotes the set of nodes as $Q_N = \{\mathbf{x}_0, \mathbf{x}_1, \ldots, \mathbf{x}_N\} = \{\mathbf{x}_\alpha\}_{\alpha=0}^{N}$. Consider next a set of functions $S_N = \{\varphi_\alpha(\mathbf{x})\}_{\alpha=1}^{N}$, each of which having the corresponding cloud ω_α as its compact support. If each one of these functions is such that $\varphi_\alpha(\mathbf{x}) \in C_0^k(\omega_\alpha)$, $k \geqslant 0$ and $\sum_{i=1}^{N} \varphi_\alpha(\mathbf{x}) = 1$, $\forall \mathbf{x} \in \Omega$, and all compact subset of Ω intersects only a finite number of supports, the set $\{\varphi_\alpha(\mathbf{x})\}$, $\alpha = 1, \ldots, N$ is said to be a partition of unity subordinated to the covering $\Im_N$. The first requirement indicates that the function φ_α is non-zero only over its respective cloud ω_α and is, at least, k times continuously differentiable.

Let $\chi_\alpha(\omega_\alpha) = \text{span}\{L_{i\alpha}\}_{i\in\mathcal{I}(\alpha)}$ denote the local function subspaces defined on ω_α, $\alpha = 1, \ldots, N$, where $\mathcal{I}(\alpha)$, $\alpha = 1, \ldots, N$, are index sets and $\{L_{i\alpha}\}_{i\in\mathcal{I}(\alpha)}$ is a set of enrichment functions for this cloud. Without loss of generality, the considered sets $\{L_{i\alpha}\}_{i\in\mathcal{I}(\alpha)}$, $\alpha = 1, \ldots, N$, are the polynomial basis functions satisfying

$$\mathcal{P}_p(\omega_\alpha) \subset \chi_\alpha^p(\omega_\alpha) \tag{2}$$

where $\mathcal{P}_p$ denotes the space of polynomials of degree less or equal to p, e.g.,

- linear basis: $\{1, (x - x_\alpha), (y - y_\alpha)\}$ or
- quadratic basis: $\{1, (x - x_\alpha), (y - y_\alpha), (x - x_\alpha)^2, (x - x_\alpha)(y - y_\alpha), (y - y_\alpha)^2\}$.

The approximation functions of a cloud ω_α are defined to be

$$\phi_{\alpha i} := \varphi_\alpha L_{i\alpha}, i \in \mathcal{I}(\alpha) \quad \text{(no sum on } \alpha\text{)}$$

Different choices of partition of unity functions are possible leading to different types of shape functions. The C^k finite element-based partitions of unity here described shares features of both standard finite element (regarding domain partition and integration procedure) and Shepard POU.

2.1 Standard finite element partition of unity

The linear triangular finite element shape functions is an example of a POU. In this case, the cloud, ω_α, is the union of the elements which share the same vertex node $\mathbf{x}_\alpha$. Hence, each node is associated with its cloud, as depicted in Fig. 1. The cloud ω_1 is a convex cloud made of the elements g, h, i, j, k and l, while the cloud ω_2, including the elements a, b, c, f, g and h is a non-convex one. The function φ_α is the same global FEM shape function. They are computationally inexpensive and easily integrated by numerical quadrature. On the other hand, their continuity is limited to C^0. This is the reason why many engineers use Reissner and Mindlin plate models even for thin plates, in spite of the locking and spurious energy modes which must be properly treated, instead of the Kirchhoff model [29].

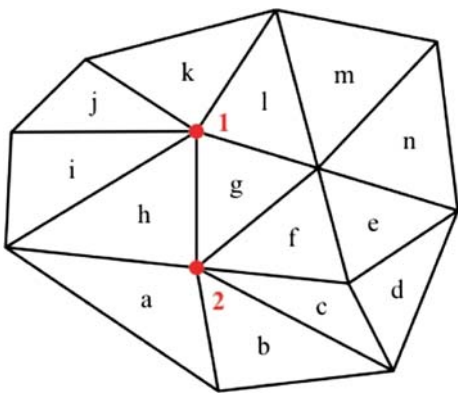

Fig. 1 Examples of convex and non-convex clouds

2.2 Shepard partition of unity

Shepard [20,42] proposed a very simple and general approach to build partition of unity functions that became widely used in meshfree methods like, e.g., *hp*-clouds [21], RKPM [32], finite spheres [14], the particle-partition of unity [28], among others. The basic concepts are reviewed in this subsection.

Let $\mathcal{W}_\alpha$:$\mathcal{R}^2 \to \mathcal{R}$ denote a *weighting function* with compact support ω_α which belongs to the space $C_0^k(\omega_\alpha)$. Assume that such a weighting function is built at every cloud ω_α, $\alpha = 1, \ldots, N$ of an open covering $\Im_N$ of the domain Ω.

The Shepard partition of unity functions subordinated to the covering $\Im_N$ is defined as

$$\varphi_\alpha(\mathbf{x}) = \frac{\mathcal{W}_\alpha(\mathbf{x})}{\sum_{\beta(\mathbf{x})} \mathcal{W}_\beta(\mathbf{x})} \quad \beta(\mathbf{x}) \in \left\{\gamma \mid \mathcal{W}_\gamma(\mathbf{x}) \neq 0\right\}, \tag{3}$$

for $\alpha = 1, \ldots, N$. Therefore, the regularity of this partition of unity depends only on the regularity of the weighting functions and, for using the Kirchhoff plate model, one needs at least functions belonging to $C^1(\Omega)$. This is known as the Shepard's scheme to define a partition of unity, and it is adopted in this work.

3 Enrichment of the approximation functions

The aim of adaptive procedures is to improve the quality of the numerical results by means of adequate enrichment of the basis of approximation subspace. The most efficient alternative for enriching the partition of unity consists of multiplying these functions by other ones such as polynomials, harmonic functions or even functions which are part of the solution of the boundary value problem as in the *hp*-clouds method. If the Shepard's functions, $\varphi_\alpha(\mathbf{x})$, are used, this procedure generates a $\mathcal{F}_N^p$ family of functions schematically shown in the following expression:

$$\mathcal{F}_N^p = \begin{Bmatrix} \varphi_1 L_{01} & \varphi_2 L_{02} & \cdots & \varphi_N L_{0N} \\ \varphi_1 L_{11} & \varphi_2 L_{12} & \cdots & \varphi_N L_{1N} \\ \vdots & \vdots & \ddots & \vdots \\ \varphi_1 L_{p1} & \varphi_2 L_{p2} & \cdots & \varphi_N L_{pN} \end{Bmatrix} \tag{4}$$

In this expression, N is the number of clouds and p is the order of the highest complete polynomial space spanned by $\mathcal{F}_N^p$. For example, let Ls_T, $T = 0, 1, 2, \ldots, M$, be the family generated by the combination of all the terms of the tensor product in $\Re^2$ of polynomials:

$$Ls_T = L_i(x_1)L_j(x_2), \quad 0 \leq i, j \leq p, \tag{5}$$

where L_m is a polynomial of degree m in $\Re$ and $T = p = i + j$. For the unidimensional case, the enrichment Ls_T, is here given by the set of polynomials

$$Ls = \{L_0, L_1, \ldots, L_p\} \tag{6}$$

and the set $\mathcal{F}_N^p$ is a space formally defined as

$$\mathcal{F}_N^p = \{\{\varphi_\alpha(x)\} \cup \{\varphi_\alpha(x) Li(x)\} : 0 \leq \alpha \leq N; \quad 0 \leq i \leq p, \quad p \geq k\}. \tag{7}$$

If the elements of the POU and the enrichment family are linearly independent, so are the elements of the set $\mathcal{F}_N^p$. This property is demonstrated in reference [21].

It is important to point out that other sets of functions such as generalized harmonic functions, anisotropic functions as well as singular solutions of the specific problem to be analyzed, can be used for enrichment purposes [17]. Also, one may enrich the approximation functions space only locally, in an adaptive scheme.

4 Weighting functions

4.1 The choice of the weighting functions

In this section, the weighting function $\mathcal{W}_\alpha$ is selected in order to satisfy some conditions which will impart great influence on the approximation process. Firstly, they must have at least the desired continuity k. Secondly, they should have reasonable integrability properties. Additionally, they must have adequate continuity as explained in [41]. In the next subsections one presents a simple form of C^∞ POU functions for convex clouds followed by an enhancement to render them applicable to non-convex clouds. This generalization is achieved by restricting the functions to be C^k, $k \geqslant 0$, with k an arbitrary integer.

4.2 C^∞ Finite element-based weighting functions for convex clouds

A C^∞ finite element-based weighting functions over convex supports can be built from the product of the so-called *cloud edge functions*. Consider first the case of an *interior convex cloud*, which is a cloud associated to an internal node (like node 1 in Fig. 2). In this case, the cloud boundary is the polygonal built from the edges of the elements in the cloud that are not connected to its node. Associated with each edge j at the boundary of a cloud ω_α, one defines a normal coordinate ξ_j, Fig. 2, which is the distance from the point P at global coordinate $\mathbf{x}$ to the edge j. Therefore it is given by

$$\xi_j(\mathbf{x}) = \mathbf{n}_{\alpha,j} \cdot \left(\mathbf{x} - \mathbf{b}_{\alpha,j}\right) \tag{8}$$

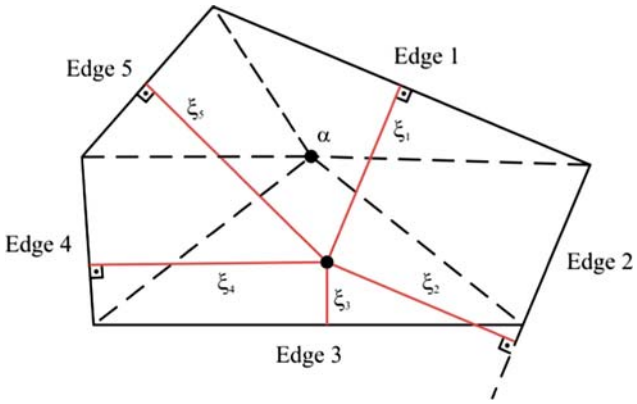

Fig. 2 Illustration of a cloud ω_α built by five triangular elements

where $\mathbf{b}_{\alpha,j}$ is a boundary point which is selected to be the midpoint of the edge j, and $\mathbf{n}_{\alpha,j}$ is the unit vector normal to this edge, pointing toward the interior of the cloud. Next, one chooses as a *cloud edge function* a function which vanishes smoothly as the edge is approached and is positive on the cloud support. Many functions can be used and the one proposed by Edwards [24,25] is adopted here resulting in C^∞ continuity. One starts with the following function

$$\varepsilon_{\alpha,j}\left[\xi_j(\mathbf{x})\right] = \widehat{\varepsilon}_{\alpha,j}(\mathbf{x}) := \begin{cases} e^{-\xi_j^{-\gamma}} & \text{if} \quad 0 < \xi_j \\ 0, & \text{otherwise} \end{cases} \tag{9}$$

where γ is a positive real constant yet to be specified.

For building the cloud weighting function, Edwards defined it as

$$\mathcal{W}_\alpha(\mathbf{x}) := e^{c_\alpha} \prod_{j=1}^{M_\alpha} \varepsilon_{\alpha,j}\left(\xi_j\right) \tag{10}$$

where M_α is the number of cloud edge functions associated with the cloud ω_α and c_α is a scaling parameter selected for each node such that $\mathcal{W}_\alpha(\mathbf{x}_\alpha) = 1$. Next, we follow a development which leads to a numerical implementation a little simpler than that presented by Edwards.

Associated with each edge j at the boundary of a cloud ω_α, one defines the height $h_{\alpha,j}$ as the normal distance of the cloud node α to the edge j, i.e.

$$h_{\alpha,j} = \xi_j(\mathbf{x}_\alpha) = \mathbf{n}_{\alpha,j} \cdot \left(\mathbf{x}_\alpha - \mathbf{b}_{\alpha,j}\right). \tag{11}$$

Scaling of the cloud edge functions is very important to prevent then from varying greatly from cloud to cloud. Numerical experiments show that it is important to have edge functions of similar shapes for all edges associated with a given cloud node, i.e., a given weighting function, regardless of the number of edges, or the height $h_{\alpha,j}$ of each one. One propose two restrictions to be satisfied by all cloud edge functions:

a. To be unitary on the cloud node: $\widehat{\varepsilon}_{\alpha,j}(\mathbf{x}_\alpha) = 1$, or $\varepsilon_{\alpha,j}(h_{\alpha,j}) = 1$. As a consequence, the weighting function is automatically unitary there too, i.e., $c_\alpha = 0$ in Eq. 10.
b. The rate of decay of all cloud edge functions is controlled by a parameter β defined by

$$\beta = \frac{\varepsilon_{\alpha,j}\left(\frac{h_{\alpha,j}}{2}\right)}{\varepsilon_{\alpha,j}\left(h_{\alpha,j}\right)} \tag{12}$$

In order to achieve these two restrictions, the cloud edge function (9) is redefined with the introduction of two new parameters, A and B, as

$$\varepsilon_{\alpha,j}\left[\xi_j(\mathbf{x})\right] = \begin{cases} A\, e^{-(\xi_j/B)^{-\gamma}} & \text{if } \xi_j > 0, \\ 0 & \text{otherwise} \end{cases} \tag{13}$$

From Eq. 12 and utilizing Eq. 13 one has

$$\varepsilon_{\alpha,j}\left(h_{\alpha,j}\right) = \frac{1}{\beta}\varepsilon_{\alpha,j}\left(\frac{h_{\alpha,j}}{2}\right)$$

$$\left(\frac{h_{\alpha,j}}{B}\right)^{-\gamma} = \left(\frac{h_{\alpha,j}}{2B}\right)^{-\gamma} + \log_e \beta$$

Therefore the scaling parameter B given by

$$B = h_{\alpha,j}\left(\frac{\log_e \beta}{1-2^\gamma}\right)^{1/\gamma} \tag{14}$$

guarantees the condition (12). At the cloud node the function has the value

$$\varepsilon_{\alpha,j}\left[h_{\alpha,j}\right] = A\, e^{-\left(\frac{1-2^\gamma}{\log_e \beta}\right)^{1/\gamma}}$$

which is constant for every edge j. Imposing $\varepsilon_{\alpha,j}[h_{\alpha,j}] = 1$, one obtains

$$A = e^{\left(\frac{1-2^\gamma}{\log_e \beta}\right)^{1/\gamma}} \tag{15}$$

Therefore, the cloud edge function defined by Eq. 13, with constants A and B defined by Eqs. 15 and 14, respectively, meets conditions a and b. In the present implementation the values $\gamma = 0.6$ and $\beta = 0.3$ is used.

A similar construction is performed for the boundary nodes. In this case, the cloud weight functions are built solely from the cloud edges which do not contain the associated boundary node.

4.3 C^k finite element-based weighting functions for non-convex clouds

It should be mentioned that the function $\mathcal{W}_\alpha(\mathbf{x})$ as proposed by Edwards is restricted do convex clouds because, by construction, it would be zero for areas inside the cloud if it were defined with non-convex support as illustrated in Fig. 3.

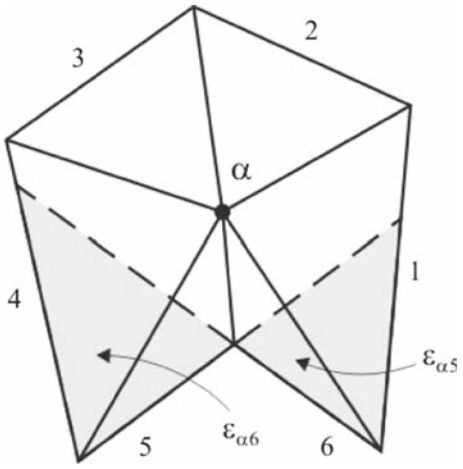

Fig. 3 Non-convex cloud where the Edwards functions are null at the hatched areas

In order to extend the applicability of Edwards weight functions (13) for non-convex clouds, Duarte [18] proposed a procedure, based on R-functions, to deal with two consecutive non-convex cloud edges. Toward this end, let one consider the R-function "*or*" with two arguments, f_1 and f_2, denoted by $(f_1 \vee_0^k f_2)$

$$\left(f_1 \vee_0^k f_2\right) := \left(f_1 + f_2 + \sqrt{f_1^2 + f_2^2}\right)\left(f_1^2 + f_2^2\right)^{\frac{k}{2}} \tag{16}$$

where k is a positive integer. This function is analytic everywhere except at the origin ($f_1 = f_2 = 0$), where it is at least k times differentiable, i.e., it belongs to $C^k(\Omega)$ [41].

If $f_1 \geqslant 0$ and $f_2 \geqslant 0$ define two regions in $\mathcal{R}^2$, then

- $\left(f_1 \vee_0^k f_2\right) \geqslant 0$ and,
- $\left(f_1 \vee_0^k f_2\right) > 0$ if $f_1 > 0$ or $f_2 > 0$.

where the arguments, f_i, can also describe curved edges.

Let one assume that sides m and n are identified as non-convex sides for a cloud ω_α. A new cloud boundary function combining $\varepsilon_{\alpha,m}$ and $\varepsilon_{\alpha,n}$ is then defined as

$$\varepsilon^{nc}_{\alpha,mn}(\mathbf{x}) := \frac{\varepsilon_{\alpha,m}(\mathbf{x}) \bigvee_0^k \varepsilon_{\alpha,n}(\mathbf{x})}{\varepsilon_{\alpha,m}(\mathbf{x}_\alpha) \bigvee_0^k \varepsilon_{\alpha,n}(\mathbf{x}_\alpha)} \tag{17}$$

where the parameter k is chosen according to the desired degree of smoothness. The combined cloud boundary function is also scaled by its value at the cloud node $\mathbf{x}_\alpha$, such that the resulting function is unitary at node α. This combined cloud boundary function is used to build a C^k weight function in a similar fashion as in (13), but where $\varepsilon^{nc}_{\alpha,mn}(\mathbf{x})$ substitutes both $\varepsilon_{\alpha,m}(\mathbf{x})$ and $\varepsilon_{\alpha,n}(\mathbf{x})$.

A similar weighting function construction, but employing R-function as a boolean "*and*", could be used instead. That

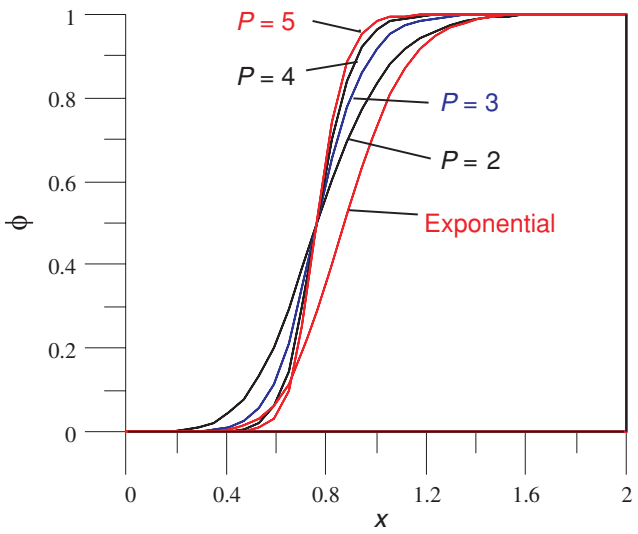

Fig. 4 Graph of the partition of unity along the line $y = 2$, associated with the central node in the mesh, for several edge functions: Exponential Eq. (13) and polynomials of degree $P = 2, 3, 4$ and 5, (cf. Eq. 11)

is, instead of (16), one could use

$$\left(f_1 \wedge_0^k f_2\right) := \left(f_1 + f_2 - \sqrt{f_1^2 + f_2^2}\right)\left(f_1^2 + f_2^2\right)^{\frac{k}{2}} \quad (18)$$

which is also at least k times continuously differentiable.

Shepard's formula, Eq. 3, is then used to build a partition of unity using the C^k weighting functions, $\mathcal{W}_\alpha(\mathbf{x})$, so obtained. This POU is therefore at least k continuously differentiable everywhere in the domain Ω and the resulting approximation functions $\mathcal{F}_N^p$ have the same continuity as long as the enrichments are also at least C^k.

4.4 C^{P-1} FEM functions with polynomial edge functions

In this paper we investigate the integrability of the finite element functions originated from cloud edge functions different from the exponential type (Eq. 13). Simple cloud edge functions can be defined by polynomials of degree P as[1]

$$\widehat{\varepsilon}_{\alpha,j}\left[\xi_j(\mathbf{x})\right] = \varepsilon_{\alpha,j}(\mathbf{x}) := \begin{cases} \left(\xi_j / h_j\right)^{\mathrm{P}} & \text{if } \ 0 < \xi_j \\ 0, & \text{otherwise} \end{cases} \quad (19)$$

where h_j is the distance from this edge to the cloud node, as defined in Eq. 11. These functions generate weighting functions with continuity C^{P-1}. Also, they are unitary in the cloud node $\mathbf{x}_\alpha$, for all edges j. Figure 4 shows the partition of unity along the line $y = 2$ for the mesh in Fig. 5a, generated from edge functions of exponential type and polynomials of degrees P = 2, 3, 4 and 5. These degrees were selected in view of the minimum continuity requirement of the most common problems in solid mechanics modeled with FEM: C^0 for Mindlin type plate bending and two- and three-dimensional solid formulations, and C^1 for Kirchhoff plate and some higher order shear models for composite laminated plate. Also, one notice that the required continuity degree is increased by one in elasticity problems if one requires continuity of stresses across element interfaces. Further, the most utilized process to extract transverse stresses in laminates, from Mindlin and Kirchhoff models, requires differentiation of the stress components in the inplane coordinates, which may suggest the use of C^2 and C^3 functions, respectively. Finally, investigations on strong residuals of the differential equilibrium equation in the Kirchhoff model requires the use of C^4 functions. In principle, the C^∞ finite element-based weighting function associated with the exponential cloud edge function would suffice. However, as will be shown in the present paper, numerical results show that each function requires different amounts of numerical effort in the element integration.

[1] One must notice that P is the degree of polynomial edge functions defined in Eq. 19, while p is the degree of cloud approximation defined in Sect. 4.

5 Kirchhoff plate model

In this section, the Kirchhoff plate model is summarized. This thin plate bending model for linear homogeneous isotropic materials, leading to a bi-harmonic equation, was first proposed by Sophie Germain in 1809 and corrected by Lagrange in 1811 [13]. It involved three boundary conditions on a free edge. Kirchhoff [29] succeeded in obtaining both the bi-harmonic Lagrange/Germain equation governing the transversal displacement and two independent boundary conditions, as required by the fourth order differential equation. This work is celebrated as the first successful application of the calculus of variations to furnish the correct and appropriate boundary conditions for a differential equation, as stated by Stoker [44].

Let us consider a region V belonging to a three-dimensional Cartesian coordinate system $\mathcal{R}^3$, defined by a constant thickness $t > 0$ and its plane middle surface Ω, which has the contour Γ. Hence, for $\mathbf{x} = \{x, y, z\}$, the region V can be described by

$$V = \left\{\mathbf{x} \in \mathcal{R}^3 \mid z \in \left[\frac{-t}{2}, \frac{t}{2}\right], (x, y) \in \Omega, \ \Omega \subset \mathcal{R}^2\right\} \quad (20)$$

In the Kirchhoff model straight normal segments to the middle surface in the undeformed state are assumed to remain straight and normal during the deformation process. Additional Kirchhoff assumptions adapted to a plate composed by orthotropic layers are: the normal stress σ_z does not affect

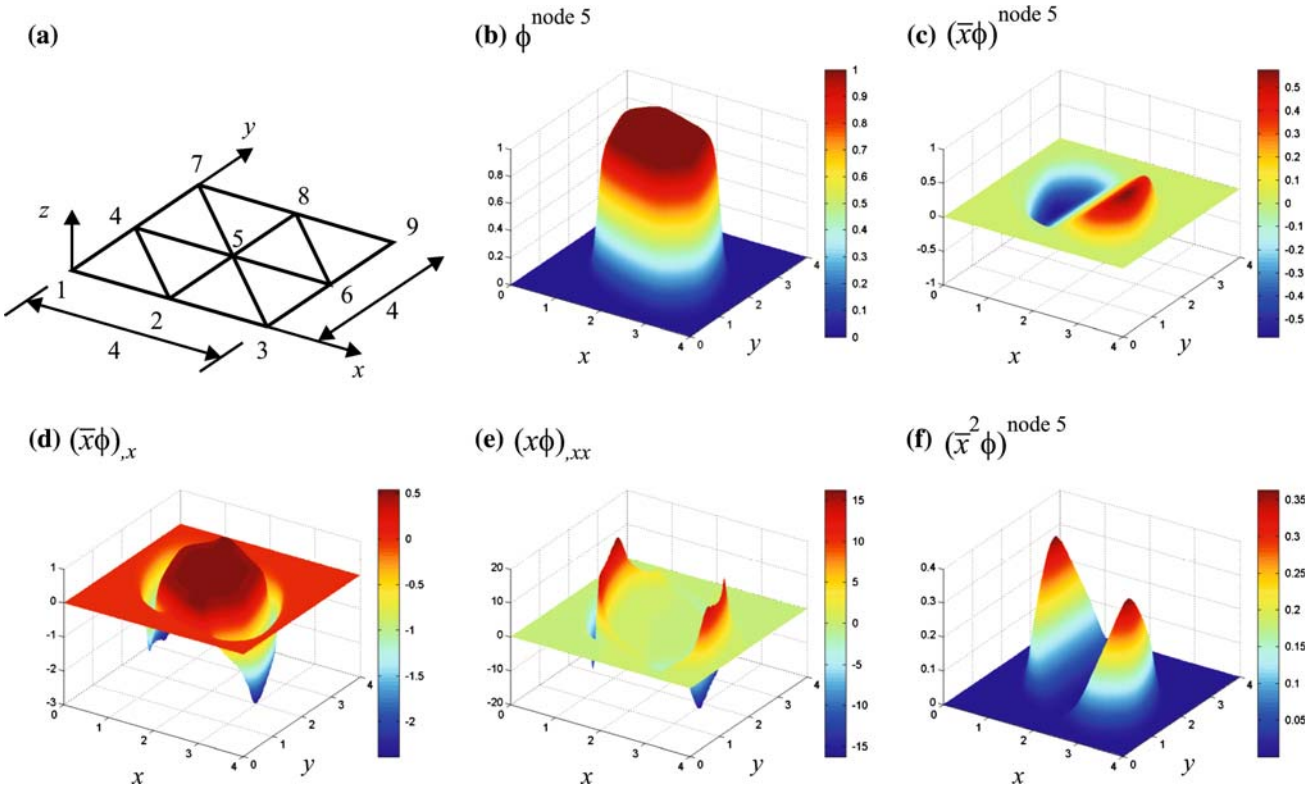

Fig. 5 Views of some enriched basis functions and its derivatives at node 5 in the mesh shown in **a**. **b** $\phi(x, y)$; **c** $\bar{x}\phi$; **d** $\partial(\bar{x}\phi)/\partial x$; **e** $\partial^2(\bar{x}\phi)/\partial x^2$; **f** $\bar{x}^2\phi$, where $\bar{x} = (x - x_{\text{node 5}})/h_5$

the deformations ϵ_{xx} and ϵ_{yy} and can be ignored; and the transversal displacements and normal rotations are very small. Under these hypothesis, the displacement field can be described as:

$$\begin{aligned} u(x, y, z) &= u^o(x, y) - \frac{\partial w}{\partial x} z \\ v(x, y, z) &= v^o(x, y) - \frac{\partial w}{\partial y} z \\ w(x, y, z) &= w(x, y) \end{aligned} \tag{21}$$

where u, v, and w stand for the displacement components along the x, y, and z directions, respectively, and u^o and v^o are inplane displacements on the middle surface. This displacement field implies the only non-vanishing linear deformation components are $\boldsymbol{\epsilon}(x, y, z) = \{\epsilon_x, \epsilon_y, \gamma_{xy}\}^T$ (the superscript T indicates transpose). These components are related to displacements by Eq. 21, resulting

$$\boldsymbol{\epsilon}(x, y, z) = \boldsymbol{\epsilon}^o(x, y) + z\boldsymbol{\kappa}(x, y), \tag{22}$$

where $\boldsymbol{\epsilon}^o$ and $\boldsymbol{\kappa}$ are the in-plane deformations and change of curvatures of the middle surface, given by $\boldsymbol{\epsilon}^o = \mathbf{L}^o \cdot \mathbf{d}$ and $\boldsymbol{\kappa} = \boldsymbol{L}^k \cdot \mathbf{d}$, where $\mathbf{L}^o$ and $\mathbf{L}^k$ are differential operators given by

$$\mathbf{L}^o = \begin{bmatrix} \frac{\partial}{\partial x} & 0 & 0 \\ 0 & \frac{\partial}{\partial y} & 0 \\ \frac{\partial}{\partial y} & \frac{\partial}{\partial x} & 0 \end{bmatrix}, \quad \mathbf{L}^k = \begin{bmatrix} 0 & 0 & -\frac{\partial^2}{\partial x^2} \\ 0 & 0 & -\frac{\partial^2}{\partial y^2} \\ 0 & 0 & -\frac{\partial^2}{\partial x \partial y} \end{bmatrix}, \tag{23}$$

and $\mathbf{d} = \{u^o, v^o, w\}^T$. The in-plane stress components are $\boldsymbol{\sigma} = \{\sigma_x, \sigma_y, \sigma_{xy}\}^T$. The Generalized Hooke's Law for an arbitrary layer k, under plane stress state, is expressed by $\boldsymbol{\sigma} = \mathbf{Q}\boldsymbol{\epsilon}$, where $\mathbf{Q}$ is the 3×3 reduced stiffness matrix representing the orthotropic layer with its principal material directions arbitrarily oriented with respect to axis x [39]. The resultant forces $\mathbf{N} = \{N_x, N_y, N_{xy}\}^T$ and resulting moments $\mathbf{M} = \{M_x, M_y, M_{xy}\}^T$ are defined as

$$\mathbf{N} = \int_{z=-t/2}^{t/2} \boldsymbol{\sigma}\, dz \text{ and } \mathbf{M} = \int_{z=-t/2}^{t/2} z\boldsymbol{\sigma}\, dz \tag{24}$$

By utilizing the reduced Hooke's Law, these definitions lead to the relation between resultant forces and moments with mid-surface deformation for the laminate

$$\begin{Bmatrix} \mathbf{N} \\ \mathbf{M} \end{Bmatrix} = \begin{bmatrix} \mathbf{A} & \mathbf{B} \\ \mathbf{B} & \mathbf{D} \end{bmatrix} \begin{Bmatrix} \boldsymbol{\epsilon}^o \\ \boldsymbol{\kappa} \end{Bmatrix} \tag{25}$$

where $\mathbf{A}$, $\mathbf{D}$ and $\mathbf{B}$ are 3×3 stiffness matrices, symmetric, representing in-plane, bending and stretch-bending coupling behavior, respectively, of the laminated plate.

In case the laminate is symmetric with respect to its middle surface, the coupling stiffness matrix $\mathbf{B} = \mathbf{0}$ and the bending response is decoupled from the in-plane behavior. The equilibrium equations in bending are

$$\begin{aligned} &\frac{\partial Q_x}{\partial x} + \frac{\partial Q_y}{\partial y} + q = 0 \\ &\frac{\partial M_x}{\partial x} + \frac{\partial M_{xy}}{\partial y} - Q_x = 0 \\ &\frac{\partial M_y}{\partial y} + \frac{\partial M_{xy}}{\partial x} - Q_y = 0 \end{aligned} \tag{26}$$

where $q(x, y)$ is the transverse applied load and Q_x and Q_y are shear forces resultants. These shear forces can be eliminated from the first equation by using the remaining ones. In the most particular case, the plate is homogeneous and isotropic, such that resulting moments in the first equilibrium equation is eliminated in terms of the curvatures using Eq. 25 and further, with operator $\mathbf{L}^k$ these can be expressed in terms of displacement only, resulting the well-known differential equation for the Kirchhoff plate bending model, for a isotropic-homogeneous and constant thickness plate:

$$\frac{\partial^4 w\,(x, y)}{\partial x^4} + 2\frac{\partial^4 w\,(x, y)}{\partial x^2 \partial y^2} + \frac{\partial^4 w\,(x, y)}{\partial y^4} = \frac{q}{D} \tag{27}$$

or, $\nabla^4 w(x, y) = q/D$, where $D = \frac{E\, t^3}{12(1-\nu^2)}$ is the bending stiffness modulus of the homogeneous isotropic plate.

The formulation implemented in this paper is aimed at the general case of laminated plates composed of anisotropic layers, represented by Eq. 25. Therefore, let us define the bilinear and linear operators

$$\begin{aligned} G(\mathbf{d}, \delta\mathbf{d}) &= \int\int_\Omega \begin{Bmatrix} \delta\epsilon^o \\ \delta\kappa \end{Bmatrix}^T \begin{bmatrix} \mathbf{A} & \mathbf{B} \\ \mathbf{B} & \mathbf{D} \end{bmatrix} \begin{Bmatrix} \epsilon^o \\ \kappa \end{Bmatrix} dxdy \\ l(\delta w) &= \int\int_\Omega \delta w\; q\; dx\, dy \end{aligned} \tag{28}$$

Hence, the plate problem can be stated in a weak form as: Find $u(x, y) \in \mathcal{U}_1$, $v(x, y) \in \mathcal{U}_1$ and $w(x, y) \in \mathcal{U}_2$ such that $G(\mathbf{d}, \delta\mathbf{d}) = l(\delta w)$, for $\forall\ \delta u^o \in \mathcal{V}_1, \forall\ \delta v^o \in \mathcal{V}_1$ and $\forall\ \delta w \in \mathcal{V}_2$, where $\mathcal{U}_1 \subset \mathcal{H}^1(\Omega)$ and $\mathcal{U}_2 \subset \mathcal{H}^2(\Omega)$ are sets of kinematically admissible functions $\mathcal{V}_1 \subset \mathcal{H}^1(\Omega)$ and $\mathcal{V}_2 \subset \mathcal{H}^2(\Omega)$ are the spaces of admissible variation fields. $\mathcal{H}^1$ and $\mathcal{H}^2$ are Hilbert spaces of order one and two, respectively, in which all functions, together with its derivatives up to first and second order, respectively, are Lebesgue square integrable.

The kinematic boundary conditions are the transversal displacement $w(x, y)$ and its normal derivative, $\frac{\partial w}{\partial n}$, and the natural boundary conditions are bending moment, M_n, and effective transversal shear stress resultant $Q_n + \frac{\partial M_{ns}}{\partial s}$, where n and s stand for outer normal and tangent local directions, respectively. Therefore, a conforming finite element requires that the displacement field $w(x, y)$ must belong to C^1 space. In the present implementation, this can be easily met at the boundaries by using the POU together with linear enrichments along the tangential and normal directions and, then, the boundary conditions can be applied as in conventional FEM.

The discretization is performed at the element level by approximating the displacement field $\mathbf{d}(x, y)$ by $\mathbf{d} = \bar{\mathbf{N}}(x,y)\, \mathbf{d}^e$, where $\mathbf{d}^e$ is the vector containing the element degrees of freedom and $\bar{\mathbf{N}}(x, y)$ is the matrix of approximation functions. The deformations of the middle surface are discretized from Eqs. (22) to (23), which result in

$$\begin{Bmatrix} \boldsymbol{\epsilon}^o \\ \boldsymbol{\kappa} \end{Bmatrix} = \begin{bmatrix} \mathbf{B}^o \\ \mathbf{B}^k \end{bmatrix} \mathbf{d}^e \quad \text{and} \quad \begin{Bmatrix} \mathbf{B}^o = \mathbf{L}^o \bar{\mathbf{N}} \\ \mathbf{B}^k = \mathbf{L}^k \bar{\mathbf{N}} \end{Bmatrix} \tag{29}$$

where $\mathbf{B}^o$ and $\mathbf{B}^k$ are the in-plane and bending strain matrices, respectively. The element stiffness matrix is evaluated in the standard way by

$$\mathbf{K}_E = \int\int [\mathbf{B}]^t\, [\mathbf{D}_K]\, [\mathbf{B}]\, J\; d\xi\; d\eta \tag{30}$$

where J stands for the Jacobian. After superposing the element stiffness matrices and consistent element load vectors, the equilibrium equations for static problems reduces to $\mathbf{K}\bar{\mathbf{u}} = \mathbf{f}$, where $\mathbf{K}$ is the global stiffness matrix, $\bar{\mathbf{u}}$ is the global degrees of freedom vector and $\mathbf{f}$ is the equivalent nodal load vector. After solving for $\bar{\mathbf{u}}$, one can compute displacements, strain, stresses and resultant forces and moments.

In this paper, all the enrichments are of polynomial type. For scaling purposes, let us define the cloud radius h_α as the largest distance from the node $\mathbf{x}_\alpha$ to each of the cloud ω_α edges. That is, consider a node $\mathbf{x}_\alpha$ and its approximation functions $\phi_i^\alpha = \varphi_\alpha(\mathbf{x}) L_{i\alpha}(\bar{\mathbf{x}})$, $i \in I(\alpha)$ where $\bar{\mathbf{x}}$ is the intrinsic coordinate defined as $\bar{\mathbf{x}} = (\mathbf{x} - \mathbf{x}_\alpha)/h_\alpha$. The enrichment sets considered are the following:

$$\begin{aligned} &\text{Quadratic:} \quad L_{i\alpha} = \left[1, \bar{x}, \bar{y}, \quad \bar{x}^2, \bar{x}\bar{y}, \bar{y}^2\right] \\ &\text{Cubic:} \quad\quad L_{i\alpha} = \left[1, \bar{x}, \bar{y}, \quad \bar{x}^2, \bar{x}\bar{y}, \bar{y}^2, \right. \\ &\qquad\qquad\qquad \left. \bar{x}^3, \bar{x}^2\bar{y}, \bar{x}\bar{y}^2, \bar{y}^3\right] \\ &\text{Quartic:} \quad L_{i\alpha} = \left[1, \bar{x}, \bar{y}, \quad \bar{x}^2, \bar{x}\bar{y}, \bar{y}^2, \right. \\ &\qquad\qquad\qquad \bar{x}^3, \bar{x}^2\bar{y}, \bar{x}\bar{y}^2, \bar{y}^3, \\ &\qquad\qquad\qquad \left. \bar{x}^4, \bar{x}^3\bar{y}, \bar{x}^2\bar{y}^2, \bar{x}\bar{y}^3, \bar{y}^4\right] \end{aligned} \tag{31}$$

The linear enrichment is the starting point for meeting the displacement normal derivative boundary conditions, but it cannot represent a constant curvature state. Thus, the quadratic enrichment generates the first useful approximation function set.

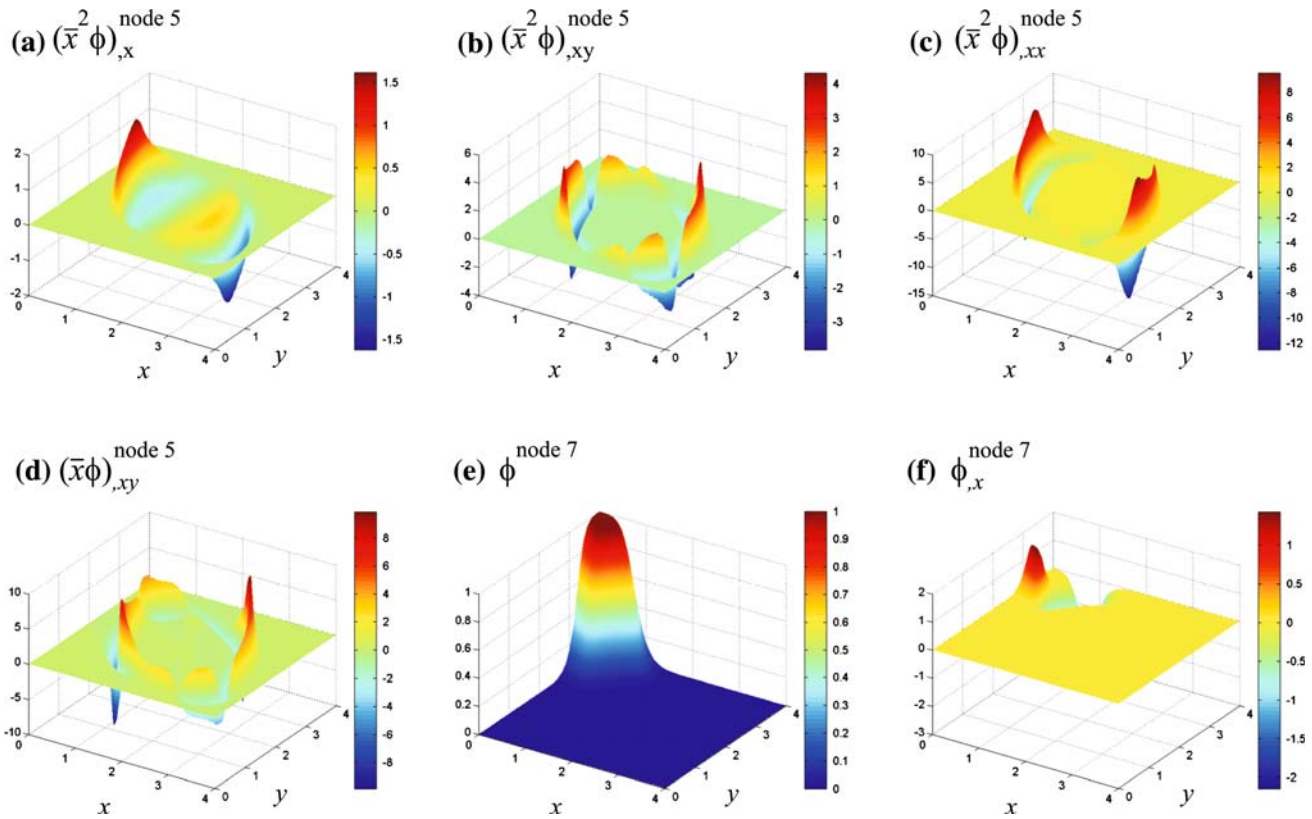

Fig. 6 Views of some enriched basis functions and its derivatives, associated with the mesh shown in Fig. 5a. For node 5: **a** $\partial(\bar{x}^2\phi)/\partial x$; **b** $\partial^2(\bar{x}^2\phi)/\partial x\partial y$; **c** $\partial^2(\bar{x}^2\phi)/\partial x^2$; **d** $\partial^2(\bar{x}\phi)/\partial x\partial y$, where $\bar{x} = (x - x_{\text{node 5}})/h_5$. For node 7: **e** $\phi(x, y)$; **f** $\partial(\phi)/\partial x$

Figures 5 and 6 show some of the enriched functions and some of their derivatives over two typical clouds, one interior, cloud 5, and one at a corner, cloud 7, of the mesh shown in Fig. 5a. These and other views qualitatively show the complexity of the surfaces associated with the derivatives of the enriched functions. The simplest form of the partition of unity on cloud 5, shown in Fig. 5b becomes more complex when it is multiplied by $\bar{x} = (x - x_5)/h_5$, as shown in Fig. 5c. Its first and second x derivatives are shown in Fig. 5d, e, where one can see the wide flat plateaus and deep sharp valleys. The same general behavior is observed with other functions and their differentials, some of which are shown in Fig. 6. The functions were obtained from the exponential edge function, and are, therefore, C^∞ functions on convex clouds. This implies that all their normal derivatives are null along the edges of the cloud. Observing, for instance, cloud 5, function ϕ is equal to one at node 5 and zero along the edge between nodes 6 and 8, in the same way required by any C^0 family of interpolation functions. However, the present family also have all normal derivatives null along that line. This generates a wide plateau with value close to zero extending close to that line, inwardly. Function ϕ drops in high gradient from value 1 to zero as shown in Fig. 5b. The level of steep oscillations of each function directly defines the amount of effort required in the numerical integration of the finite element matrices.

Functions ϕ with different behaviors can be obtained from different types of edge functions utilized in the generation of the weighting functions. Figure 4 shows a graph for ϕ associated with an internal node, obtained from exponential and polynomial edge functions. Clearly, only the exponential one generates C^∞ approximation functions. Still, it is the most smooth function compared with those based on polynomial edge functions. Only the second degree polynomial edge function generates ϕ with similar shape as the exponential one. This is also identified from the numerical experiments shown in the next section. Consistently, those results show that functions based on these two functions are the most easily integrated.

6 Numerical results

In order to assess the performance and identify characteristic behaviors of the model described, some typical problems of thin laminated plates are analyzed. The results obtained are compared with those obtained from analytical solution based on thin laminated plate theory [47]. In all cases, only bending behavior is considered, with symmetric laminates under transverse distributed load. However, the model is equally adequate to general non-symmetric laminates.

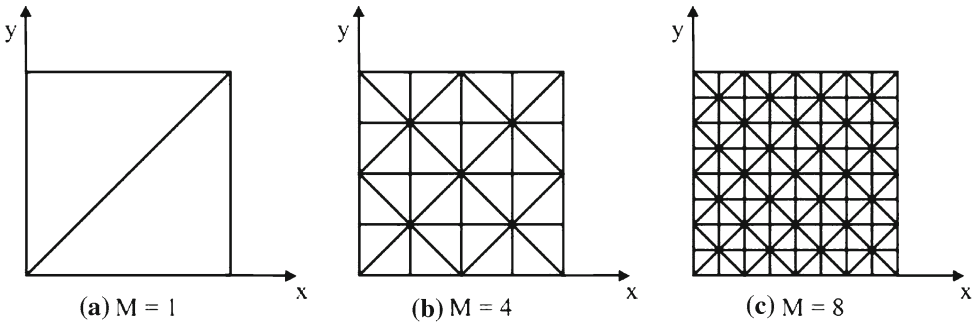

Fig. 7 Some meshes utilized in the square laminated plate problem. Examples of mesh indices $M = 1, 4$ and 8

The formulation is numerically implemented on partition of the plate domain in triangular elements with three nodes and straight edges. The stiffness matrix, although non-singular, become ill-conditioned when enriched with higher order polynomials. In the present work, the $\mathbf{K}_\epsilon$ scheme is adopted, following [17].

6.1 Square laminated plate

A simply supported square plate is modeled, with equal sides a and b along x and y directions, respectively, and thickness t, with $a/t = 4$, and three equal orthotropic layers with orientations $[0°/90°/0°]$ with respect to axis x. Each layer has the following properties in its orthotropic directions:

$$E_1 = 175 \text{ GPa} \quad G_{12} = 3.5 \text{ GPa}$$
$$E_2 = 7 \text{ GPa} \quad \nu_{12} = 0.25$$

A normal distributed load is applied, varying as $q(x, y) = q_o \sin \pi x/a \sin \pi y/b$. The uniform meshes are identified by an index M, whose definition is illustrated in Fig. 7 for $M = 1, 4$ and 8, along with the global coordinate axis.

The boundaries are simply supported, such that the following conditions have to be imposed:

$$\begin{aligned} w = \frac{\partial w}{\partial y} = \frac{\partial^2 w}{\partial y^2} = \cdots = 0 \qquad & \text{for } x = \text{const.} \\ w = \frac{\partial w}{\partial x} = \frac{\partial^2 w}{\partial x^2} = \cdots = 0 \qquad & \text{for } y = \text{const.} \end{aligned} \tag{32}$$

The need for imposition of higher order derivatives on the boundaries is due to the presence of higher non-zero derivatives present in the approximation functions, which are inherited from the characteristics of the selected cloud edge functions.

The actual nodal degrees of freedom to be restricted in order to attain conditions (32) can be identified by expressing the complete expression for the transverse displacement $w(x, y)$ associated with an arbitrary node α, for the partition of unity $\phi = \phi(\bar{x}, \bar{y})$, enriched by the fourth degree polynomial (Eq. 31) as:

$$\begin{aligned} w(x, y) = {} & w_\alpha \phi + w_x (\bar{x}\, \phi) + w_y (\bar{y}\, \phi) + w_{x^2} \left(\bar{x}^2\, \phi\right) \\ & + w_{xy} (\bar{x}\bar{y}\, \phi) + w_{y^2} \left(\bar{y}^2\, \phi\right) + w_{x^3} \left(\bar{x}^3\, \phi\right) \\ & + w_{x^2y} \left(\bar{x}^2\bar{y}\, \phi\right) + w_{xy^2} \left(\bar{x}\bar{y}^2\, \phi\right) + w_{y^3} \left(\bar{y}^3\, \phi\right) \\ & + w_{x^4} \left(\bar{x}^4 \phi\right) + w_{yx^3} \left(\bar{x}^3\bar{y}\, \phi\right) + w_{x^2y^2} \left(\bar{x}^2\bar{y}^2 \phi\right) \\ & + w_{xy^3} \left(\bar{x}\bar{y}^3\, \phi\right) + w_{y^4} \left(\bar{y}^4\, \phi\right) \end{aligned} \tag{33}$$

The coefficients w_α, w_x, w_y and so on, are the nodal coefficients. The expression for w with enrichments of third and second degree polynomials are obtained truncating Eq. 33 adequately.

For clouds on boundary lines $x = \text{const.}$, one has $\bar{x} = 0$, and condition $w = 0$ makes it necessary to impose

$$w_\alpha = w_y = w_{y^2} = w_{y^3} = w_{y^4} = 0 \tag{34}$$

and for clouds on boundary lines $y = \text{const.}$, one has $\bar{y} = 0$ and it is necessary to impose

$$w_\alpha = w_x = w_{x^2} = w_{x^3} = w_{x^4} = 0 \tag{35}$$

Differentiation of $w(x, y)$ in Eq. 33, for $\partial w/\partial x$ and $\partial w/\partial y$ enables to identify the necessary coefficient restrictions to satisfy conditions (32). For instance,

$$\begin{aligned} \frac{\partial w}{\partial x} = {} & w_\alpha \bar{\phi}_{,x} + w_x \left(\phi + \bar{x}\, \bar{\phi}_{,x}\right) + w_y \left(\bar{y}\, \bar{\phi}_{,x}\right) + w_{x^2} \left(2\bar{x}\, \bar{\phi}\right. \\ & \left. + \bar{x}^2\, \bar{\phi}\right) + w_{xy} \left(\bar{y}\, \bar{\phi} + \bar{x}\bar{y}\, \bar{\phi}_{,x}\right) + w_{y^2} \left(\bar{y}^2\, \bar{\phi}_{,x}\right) \\ & + w_{x^3} \left(3\bar{x}^2\bar{\phi} + \bar{x}^3\, \bar{\phi}_{,x}\right) + w_{x^2y} \left(2\bar{x}\bar{y}\, \bar{\phi} + \bar{x}^2\bar{y}\, \bar{\phi}_{,x}\right) \\ & + w_{xy^2} \left(\bar{y}^2\, \bar{\phi} + \bar{x}\bar{y}^2\, \bar{\phi}_{,x}\right) + w_{y^3} \left(\bar{y}^3\, \bar{\phi}_{,x}\right) \\ & + w_{x^4} \left(4\bar{x}^3\, \bar{\phi} + \bar{x}^4\, \bar{\phi}_{,x}\right) + w_{yx^3} \left(3\bar{x}^2\bar{y}\, \bar{\phi} + \bar{x}^3\bar{y}\, \bar{\phi}_{,x}\right) \\ & + w_{x^2y^2} \left(2\bar{x}\bar{y}^2\, \bar{\phi} + \bar{x}^2\bar{y}^2\, \bar{\phi}_{,x}\right) \\ & + w_{xy^3} \left(\bar{y}^3\, \bar{\phi} + \bar{x}\bar{y}^3\, \bar{\phi}_{,x}\right) + w_{y^4} \left(\bar{y}^4\, \bar{\phi}_{,x}\right) \end{aligned} \tag{36}$$

where $\phi = \phi(\bar{x}, \bar{y})$, $\bar{\phi} = \phi/h_\alpha$ and $\bar{\phi}_{,x} = \frac{1}{h_\alpha} \partial\phi/\partial\bar{x} = \partial\bar{\phi}/\partial\bar{x}$. By construction, $\partial\phi/\partial x = 0$ on node α. Restriction

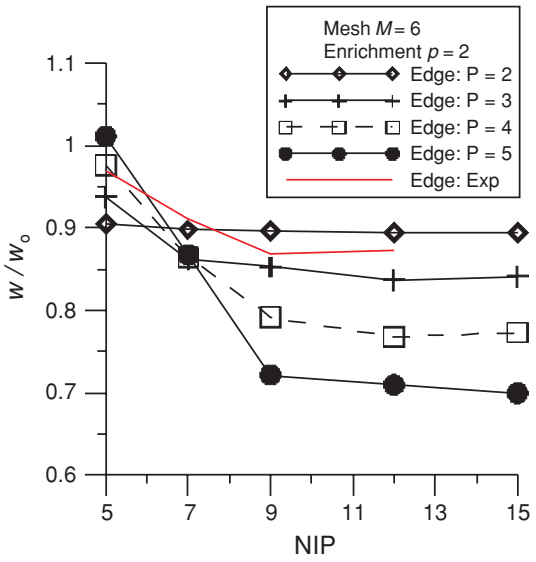

Fig. 8 Center displacement ratio versus number of integration points index NIP for several edge functions. Mesh 6×6, enrichment $p = 2$

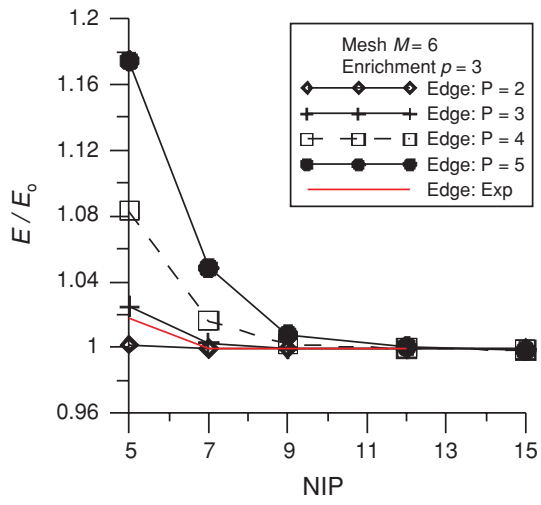

Fig. 9 Energy norm E versus number of integration points index NIP for several edge functions. Mesh 6×6, enrichment $p = 3$

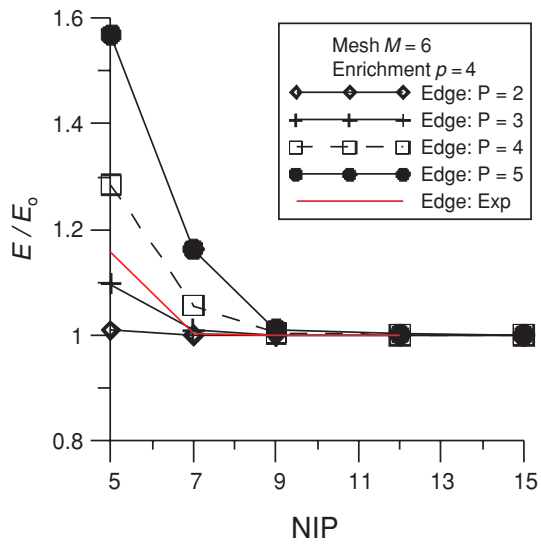

Fig. 10 Energy norm ratio versus number of integration points index NIP for several edge functions. Mesh 6×6, enrichment $p = 4$

of coefficients (35) also nullifies $\partial w/\partial x$ along boundaries $y = const$. In fact, differentiating w further, one can easily show that restrictions (35) also nullify all x derivatives of w along these borders. Analogously, restrictions (34) nullify all y derivatives of w along boundaries $x = \text{const}$.

Firstly, the overall behavior of functions generated by different types of cloud edge functions is addressed in Figs. 8, 9, 10, where five different edge functions are considered: the exponential function, Eq. (13) and the polynomial ones, of degree P, defined in Eq. (19). Central displacement w is normalized with respect to analytical displacement w_o [47]. The approximate and analytic strain energy of the plate are E and E_o, respectively. For this orthotropic symmetrical laminate with sinusoidal distributed load, analytical solution based on Kirchhoff hypothesis produce $w_o = (a/\pi)^4 q_o/\bar{D}$ and $E_o = q_o w_o ab/4$, with $\bar{D} = D_{11} + 2(D_{12} + 2D_{33})(a/b)^2 + D_{22}(a/b)^4$, and D_{ij} are components of bending stiffness matrix $\mathbf{D}$ in Eq. (25). These figures show displacement and strain energy versus NIP, the square root of the total number of Gaussian integration points in the element, for a mesh $M = 6$, with functions enriched by polynomials of degrees $p = 2, 3$ and 4. In all cases, it is observed that the convergence behavior of central displacement is similar to those for strain energy, such that only displacements for $p = 2$ are shown.

Figure 8 for enrichment polynomial $p = 2$, show that the most easily integrated functions are those based on exponential and polynomial P = 2 edge functions, which approximate the converged values with NIP somewhere below 8 with reasonable accuracy. Edge functions of degrees P = 3–5 require a greater effort in the integration process. The same behavior can be seen for enrichment polynomials $p = 3$ and 4 in Figs. 9 and 10. These figures also show the convergence of solution as the enrichment degrees grow, for all edge functions tested. Observation of this and other numerical results indicate that NIP = 9 points in Gaussian rule leads to an accurate integration for the functions based in the exponential edge function, for all enrichment polynomials tested. Approximation functions generated by the remaining types of edge functions require a larger number of integration points, except for the quadratic edge function, which can be integrated with the same effort as the exponential one. In the sections that follow, this proposition is tested under different circumstances.

Figure 11 shows the central normalized displacement ratio for different mesh indices M, for enrichments $p = 2, 3$ and 4,

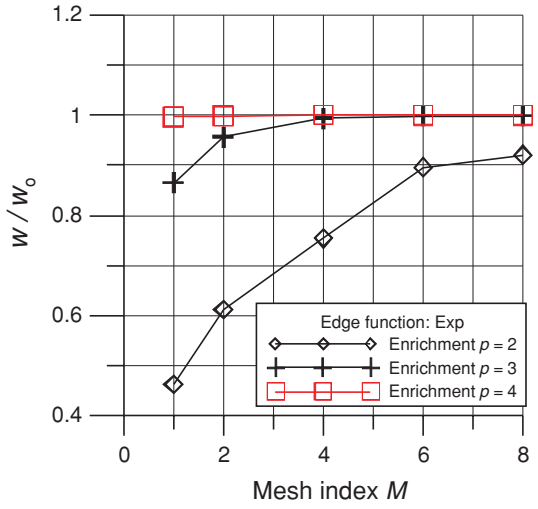

Fig. 11 Central displacement ratio for different mesh indices M, for enrichments $p = 2, 3$ and 4. Exponential edge function. Gaussian Integration Rule with NIP = 9

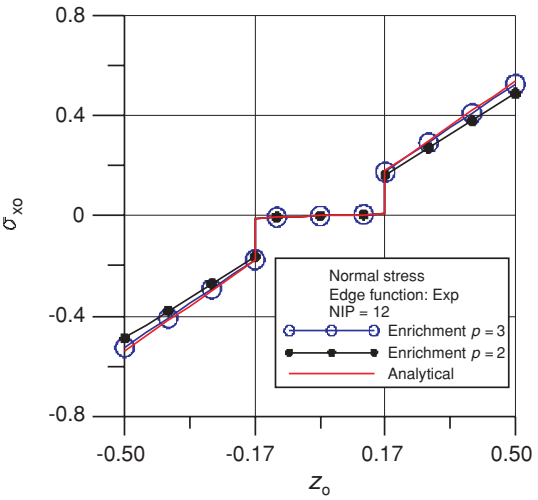

Fig. 12 Normalized in-plane normal stress $\sigma_{xo} = \sigma_x t^2/(q_o a^2)$, along thickness at $(x, y) = (0, 0)$. Normalized coordinate $z_o = z/t$. Exponential edge function, Gaussian integration rule with NIP = 12. $a/t = 4$. Mesh index $M = 6$

with partition of unity generated by exponential edge functions. The results are obtained with NIP = 9 Gaussian integration rule and illustrates the h-convergence of the method. Figure 11 shows that high accuracy in displacements can be met even by using two elements ($M = 1$) with uniform p -enrichment for this load case.

Figures 12 and 13 show the normalized in-plane normal stress σ_{xo} through the thickness at center plate, $(x, y) = (a/2, b/2)$, and normalized transverse shear stress τ_{xzo} along the thickness at coordinates, $(x, y) = (0, b/2)$. The mesh index is $M = 6$ and the functions are enriched with polynomial of degree $p = 2, 3$ and 4. The edge function is exponential, and the Gaussian integration rule is utilized with

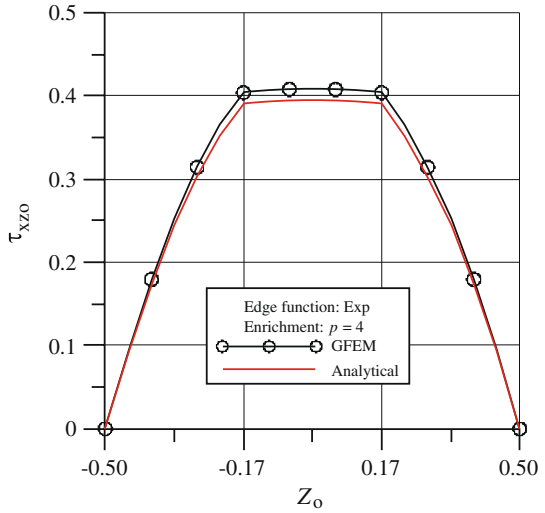

Fig. 13 Normalized transverse shear stress $\tau_{xyo} = \tau_{xy} t/(q_o a)$, along thickness at $(x, y) = (0, a/2)$. Normalized coordinate $z_o = z/t$. Exponential edge function, Gaussian integration rule with NIP = 12. $a/t = 4$. Mesh index $M = 6$

NIP = 12. The stresses and transverse coordinate are normalized according to $\sigma_{xo} = \sigma_x t^2/(q_o a^2)$, $\tau_{xyo} = \tau_{xy} t/(q_o a)$ and $z_o = z/t$, respectively. In Fig. 12 the results for enrichment $p = 4$ is too close to the analytical solution to be visible, and it is suppressed. The relative error in l_∞ norm is 0.0928% for $p = 4$. These transverse shear stresses are obtained by integration of equilibrium equations and the analytical solution is also obtained from integration of the analytical solution of the Kirchhoff model for the problem.

One verifies how important the numerical integration issue is for this class of GFEM. Unexpectedly, the use of second degree edge functions may be convenient if one is not concerned with stress continuity in element interfaces, since it requires less integration points under appropriate h and p enrichments. Otherwise, the exponential edge functions should be preferred for its computational efficiency compared with higher order polynomials.

6.2 Test with triangular integration rule

In principle, the most adequate integration rule to integrate a triangular domain is a triangular rule. However, the triangular rules available are limited in their maximum number of integration points, and hence in the largest polynomial exactly integrated by then. On the other hand, Gaussian quadratures codes are based on algorithms readily expandable to arbitrarily large number of integration points. The inherent difficulty of integration in the present formulation naturally suggests the use of Gaussian rule to asses reliable integration values of the approximate responses. In the figures that follow, these results are compared with those obtained from the Dunavant triangle integration rules [23].

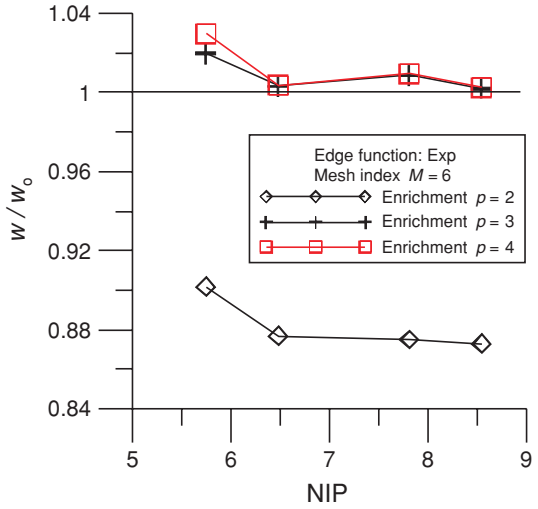

Fig. 14 Triangular integration rule. Central displacement ratio versus integration index NIP, for enrichments $p = 2, 3$ and 4, mesh index $M = 6$. Exponential edge function

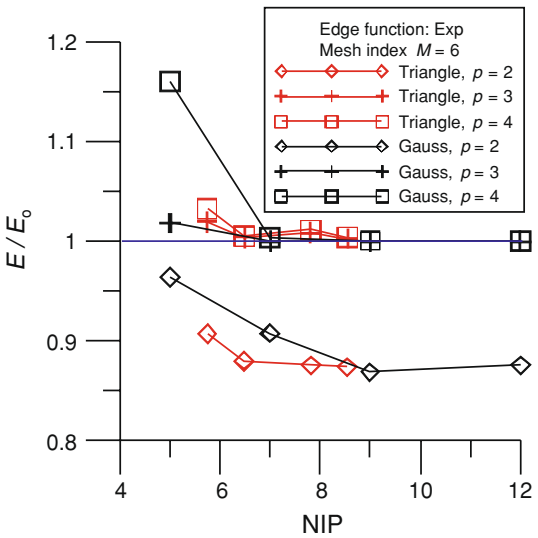

Fig. 15 Gaussian and triangular integration rules. Energy norm ratio versus integration index NIP, for enrichment polynomials $p = 2, 3$ and 4, mesh index $M = 6$. Exponential edge function. Square laminate

Figure 14 shows the central displacement ratio versus integration index NIP, obtained with the triangular integration rule, with enrichment polynomials $p = 2, 3$ and 4, mesh index $M = 6$ and exponential edge function. Figure 15 is obtained under similar conditions, but shows the energy norm ratio instead central displacement and compares results of Gaussian and triangular integration rules. The number of triangular integration points is limited to the maximum available [23], which is 73 points, (NIP = 8.54), which, in most cases tested, give result similar to those obtained with NIP = 9 Gaussian points. For certain level of accuracy, good results appear in these figures with NIP = 6.48 triangular points (more detailed discussion on the convergence integration errors is described in the next section). Similar test is represented in Fig. 16, where second degree edge function is utilized. These results also indicate similar integrability of approximation functions generated from exponential and quadratic edge functions. The integrability characteristics of the quadratic edge functions is detailed in the next section.

These results indicate that the Dunavant triangle integration rules allows good accuracy using less integration points but, contrary to Gauss-Legendre rules, it does not lead to monotonic convergence as the number of integration points is increased.

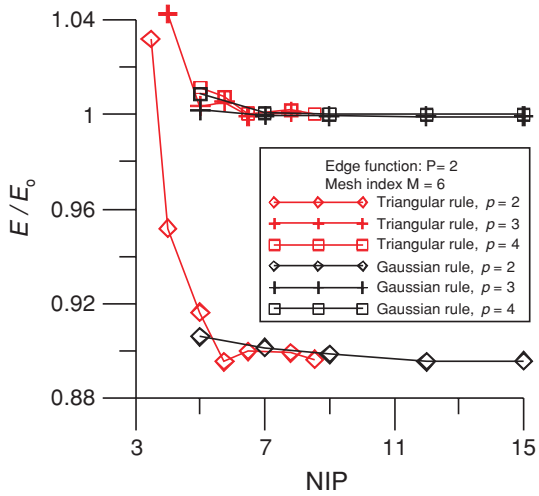

Fig. 16 Gaussian and triangular integration rules. Energy norm ratio versus integration index NIP, for enrichment polynomials $p = 2, 3$ and 4, mesh index $M = 6$. Edge function: polynomial of degree P = 2. Square laminate

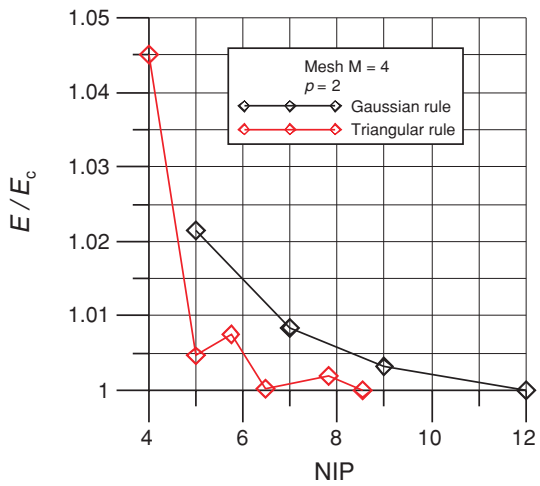

Fig. 17 Gaussian and triangular integration rules. Energy norm ratio versus integration index NIP, for enrichment polynomial $p = 2$, mesh index $M = 4$. Edge function: polynomial of degree P = 2. Rectangular laminate

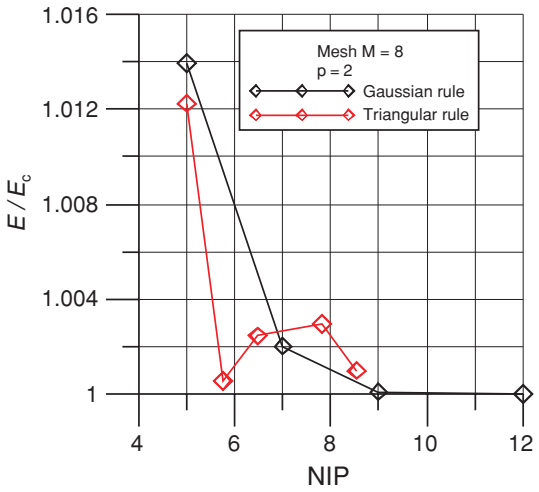

Fig. 18 Gaussian and triangular integration rules. Energy norm ratio versus integration index NIP, for enrichment polynomial $p = 2$, mesh index $M = 8$. Edge function: polynomial of degree P = 2. Rectangular laminate

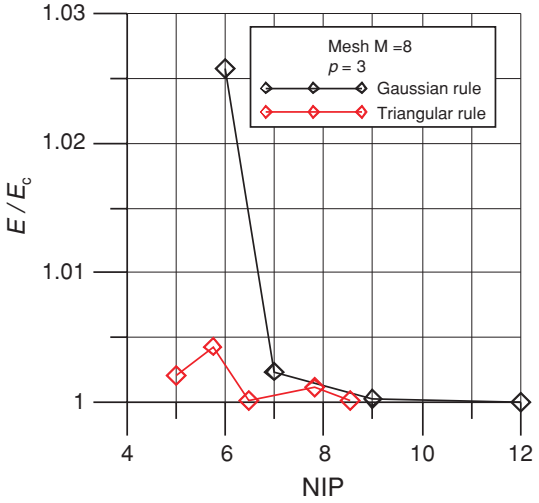

Fig. 20 Gaussian and triangular integration rules. Energy norm ratio versus integration index NIP, for enrichment polynomial $p = 3$, mesh index $M = 8$. Edge function: polynomial of degree P = 2. Rectangular laminate

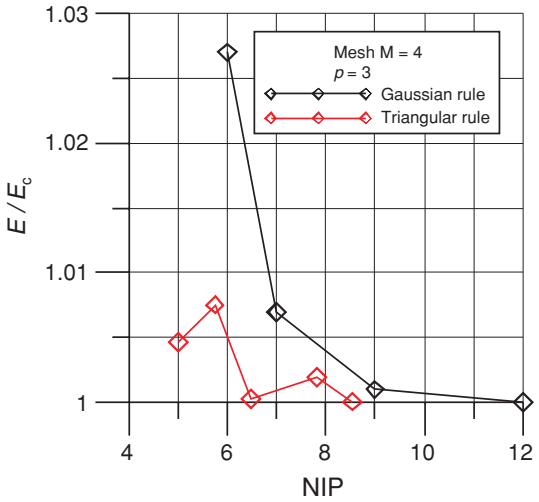

Fig. 19 Gaussian and triangular integration rules. Energy norm ratio versus integration index NIP, for enrichment polynomial $p = 3$, mesh index $M = 4$. Edge function: polynomial of degree P = 2. Rectangular laminate

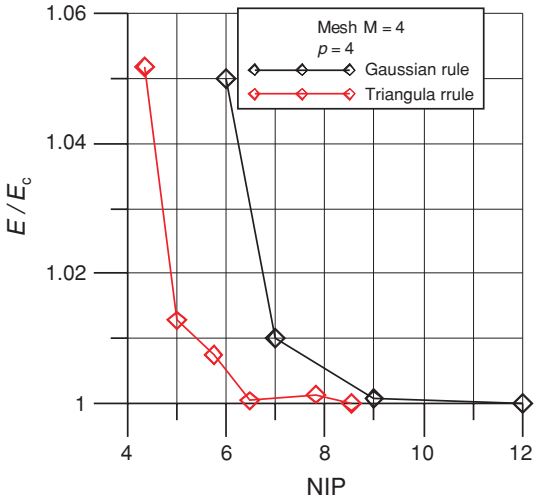

Fig. 21 Gaussian and triangular integration rules. Energy norm ratio versus integration index NIP, for enrichment polynomial $p = 4$, mesh index $M = 4$. Edge function: polynomial of degree P = 2. Rectangular laminate

6.3 Tests on edge function P = 2: rectangular laminated plate

One considers the same laminated plate of the previous section but in rectangular shape, with sides $a = 2b$. The meshes are of the same type shown in Fig. 7. Here the results are normalized with respect to a reference value obtained with NIP = 15 Gaussian integration points, being E_c such value. Therefore, the ratio E/E_c indicates integration error instead of analytical solution error. Figures 17 and 18 show comparisons of energy ratio versus integration index NIP obtained by Gaussian and triangular integration Rules. The enrichment is polynomial $p = 2$, mesh index $M = 4$ and 8 for each figure, and the edge function is the polynomial of degree P = 2. Figures 19, 20, 21 and 22 show the results obtained under the same conditions, but for enrichment polynomials $p = 3$ and 4. Firstly, one observe in all cases an asymptotic behavior of the Gaussian rule results, in opposition to the oscillatory response of triangular rule. For all enrichment degrees, triangular rule converge with NIP = 6.48 (42 points), with better or similar accuracy than Gaussian rule with the same number of points. However, in several of the cases shown, Gaussian rule give better or similar accuracy than triangular rule at NIP = 9. Finally, moderate accuracy of about 1% or

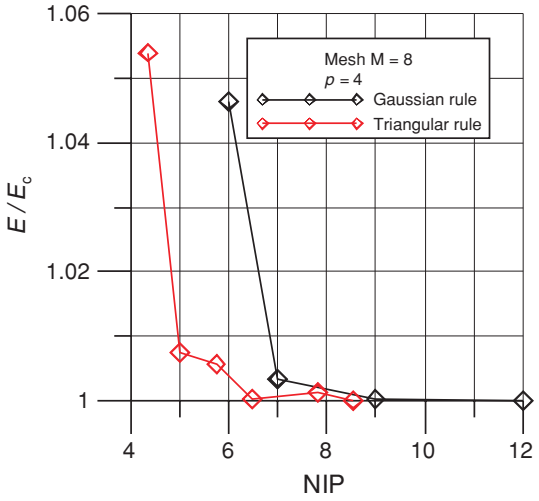

Fig. 22 Gaussian and triangular integration rules. Energy norm ratio versus integration index NIP, for enrichment polynomial $p = 4$, mesh index $M = 8$. Edge function: polynomial of degree P = 2. Rectangular laminate

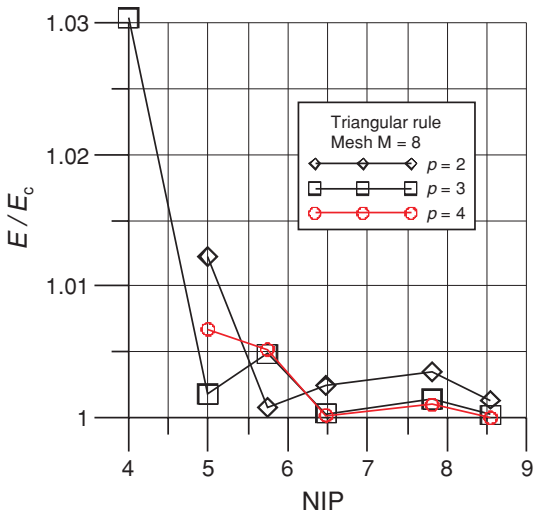

Fig. 23 Triangular integration rule. Energy norm ratio versus integration index NIP, for enrichment polynomials of degrees $p = 2$, 3 and 4. Mesh index $M = 4$. Edge function: polynomial of degree P = 2. Rectangular laminate

less can be obtained with NIP = 5 of triangular rule, for all enrichment polynomials tested. This number of points seems similar to the 4×4 Gaussian integration rule of usual bi-cubic quadrangular finite elements in C^o continuous applications like plane elasticity. It must be pointed out, however, that, in the present formulation, the integration effort seems to be unaltered by the degree of enrichment of the approximation functions utilized, as can be seen in Figs. 23 and 24, which summarize the results of the previous figures for triangular rule in meshes $M = 4$ and 8.

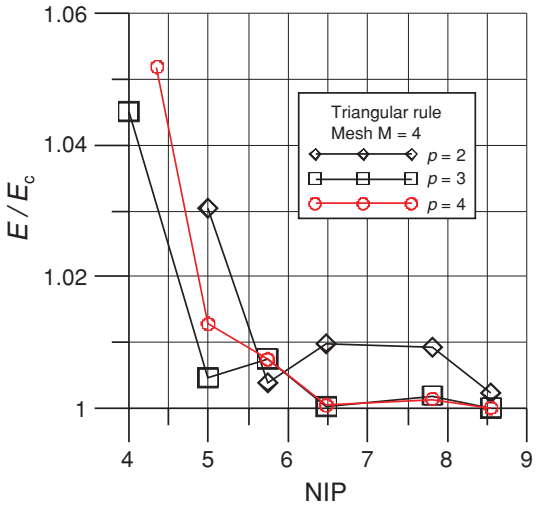

Fig. 24 Triangular integration rule. Energy norm ratio versus integration index NIP, for enrichment polynomials of degrees $p = 2$, 3 and 4. Mesh index $M = 8$. Edge function: polynomial of degree P = 2. Rectangular laminate

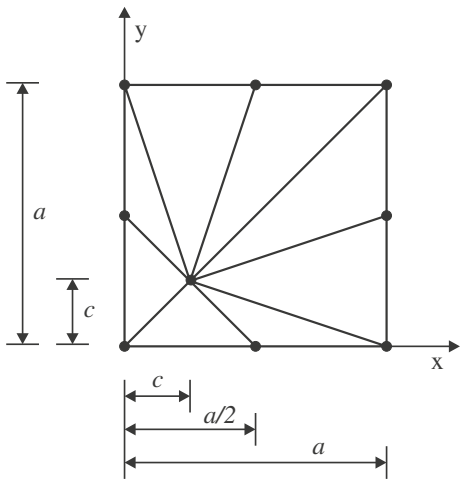

Fig. 25 Illustration of distorted mesh with $2c/a = 0.25$

6.4 Test on mesh distortion

Here the behavior of the method is tested in a more severe mesh distortion than the previous application. The regular mesh with index $M = 2$ for the square laminate problem was taken, and its central node was made to move towards the coordinate system origin. The resulting mesh is shown in Fig. 25, and it is defined by the mesh distortion ratio $2c/a$, such that $2c/a = 1$ indicates a regular mesh of the type shown in Fig. 7 and the elements distortion grows as $2c/a$ approaches zero. Figure 26 shows the variation of the relative error in energy norm against $2c/a$, for enrichment polynomial of degree $p = 4$ and polynomial edge function of degree P = 2. Results are obtained with Gaussian and triangular integration rules. In all cases, it can be observed that

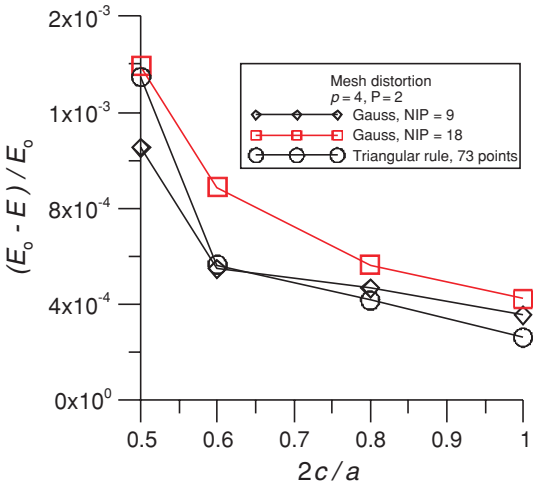

Fig. 26 Test on mesh distortion. Triangular and Gaussian integration rules. Relative error of energy norm versus mesh distortion ratio $2c/a$, for enrichment polynomial of degree $p = 4$. Mesh index $M = 2$. Edge function: polynomial of degree P = 2. Square laminate

mesh distortion causes some loss in accuracy. This is a characteristic of the methods based on partition of unity. Since the enrichment functions are defined in global coordinates, they are not quite susceptible to the mesh shape, but the partition of unity is defined in a support composed by a patch of more or less distorted elements, which renders the formulation with some mesh dependency in its accuracy in this very poorly refinement, with only one interior node.

7 Conclusions

In this paper, an arbitrarily smooth kind of Partition of Unity has been investigated under the GFEM approach for the modeling of laminated composite plate under Kirchhoff model. The procedure to build generalized finite element approximation functions has the following features:

(i) The formulation proposed was capable to approximate the solution of the Kirchhoff plate model meeting the C^k continuity requirement;
(ii) It allows higher continuity without additional effort if one is interested to have continuity in higher order derivatives to obtain continuous stress resultants;
(iii) Non-structured mesh composed of triangular elements are presently adopted.
(iv) Although the POU of this implementation for the generalized finite element shape functions can exactly reproduce polynomials up to the fourth order, higher order polynomials and non-polynomials can be used as well.
(v) The examples in this paper only considered simply supported plates, but any distributional boundary conditions can be dealt with.
(vi) The approximation functions have the same support as corresponding triangular finite element shape functions.
(vii) It is possible, with the present formulation, to obtain a continuous in-plane stress field without the need to perform smoothing operations.
(viii) With appropriate enrichment, good quality of the in-plane stresses is achieved. This, in turn, results in good estimates of the transverse shear stresses in the laminate, when compared to the values obtained by integration of equilibrium equations of the in-plane analytical stresses of the Kirchhoff model.

Although property (vi) listed above facilitates the domain numerical integration, the required number of integration points is larger than in the case of generalized finite element methods based on C^0 partitions of unity, as expected. The issue of numerical integration is presently discussed for Gaussian quadratures and for the Dunavant's rule for triangular elements, for various types of edge functions. Among these, the exponential one is the most general and with easier integration behavior together with the second order polynomial. The later one is obviously restricted to C^1 continuity, but it requires less computational effort and also leads to reasonable accuracy. In addition, it is also shown that high accuracy can be obtained in stress evaluation.

The proposed C^k functions and associated p-enrichments, in spite of presenting steep second derivatives oscillations, lead to good accuracy for both h and p refinement. This property indicates that they may be a good choice for other plate models for laminated composites which require C^1 continuity for appropriate stress computations.

Acknowledgments We gratefully acknowledge the Conselho Nacional de Desenvolvimento Cientifico e Tecnologico (CNPq) at Brazil for its support in the Research Project No. 309.640/2006-7.

References

1. Amarantuga K, Williams JR, Quan S, Weis J (1994) Wavelet-Galerkin solutions for one-dimensional partial differential equations. Int J Numer Methods Eng 37:2703–2716
2. Atluri SN, Zhu T (1998) New meshless local Petrov-Galerkin (MPLG) approach in computational mechanics. Comput Mech 22:117–127
3. Babuška I, Melenk JM (1995) The partition of unity method. Technical Note BN-1185, Institute for Physical Science and Technology, University of Maryland
4. Babuška I, Melenk JM (1996) The particion of unity finite element method: basic theory and applications. Comput Methods Appl Mech Eng 139:289–314

5. Barros FB, Proença SPB, de Barcellos CS (2004) On error estimator and *p*-adaptivity in the generalized finite element method. Int J Numer Meth Eng 60:2373–2398
6. Barros FB, de Barcellos CS, Duarte CA (2007) *p*-Adaptive C^k generalized finite element method for arbitrary polygonal clouds. Comput Mech 41:175–187
7. Beirão da Veiga L, Niiranen J, Eternberg R (2007) A family of C^0 finite element for Kirchhoff plates I: error analysis. SIAM J Numer Anal 45:2047–2071
8. Belinha J, Dinis L (2006) Elasto-plastic analysis of plates by the element free Galerkin Method. Eng Comput 23:525–551
9. Belinha J, Dinis L (2006) Analysis of plates and laminates using the element free Galerkin method. Comput Struct 84:1547–1559
10. Belytschko T, Black T (1999) Elastic crack growth in finite elements with minimal remeshing. Int J Numer Methods Eng 45: 601–620
11. Belytschko T, Liu W, Singer M (1998) On adaptivity and error criteria for mesh free methods. In: Ladèveze P, Oden JT (eds) Adv Adaptive Comput Methods Mech 217–228
12. Belytschko T, Lu YY, Gu J (1993) Crack propagation by element free Galerkin methods. In: Advanced computational methods for material modeling, AMD vol 180/PVP vol 268. ASME, New York, pp 191–205
13. Bucciarelli LL, Dworsky N (1980) Sophie Germain. An essay in the history of the theory of elasticity. Reidel, Dordrecht
14. De S, Bathe KJ (2000) The method of finite spheres. Comput Mech 25:329–345
15. Dolbow J, Moës N, Belytschko T (2000) Modeling fracture in Mindlin-Reissner plates with the extended finite element method. Int J Solids Struct 37:7161–7183
16. Donning BM, Liu WK (1998) Meshless methdos for shear-deformable beams and plates. Comput Methods Appl Mech Eng 152:47–71
17. Duarte CA, Babuška I, Oden JT (2000) Generalized finite element method for three-dimensional structural mechanics problems. Comput Struct 77:215–232
18. Duarte CA, Kim DJ, Quaresma DM (2006) Arbitrarily smooth generalized element approximations. Comput Methods Appl Mech Eng 196:33–56
19. Duarte CA, Hamzeh ON, Liska TJ, Tworzyllo WW (2001) A generalized finite element method for the simulation of three-dimensional dynamic crack propagation. Comput Methods Appl Mech Eng 190:2227–2262
20. Duarte CA, Oden JT (1995) hp Clouds—A meshless method to solve boundary value problems. TICAM report 95-05, University of Texas
21. Duarte CA, Oden JT (1996) *hp* Clouds—an *hp* meshless method. Numer Methods Partial Diff Equ 12:673–705
22. Duarte CA, Oden JT (1996) An *h-p* adaptive method using clouds. TICAM report 96-07, University of Texas
23. Dunavant DA (1985) High degree efficient symmetrical gaussian quadrature rules for the triangle. Int J Numer Methods Eng 21:1129–1148
24. Edwards HC (1996) C^∞ finite element basis functions. Technical Report, TICAM report 96-45. The University of Texas at Austin
25. Edwards HC (1997) A parallel infrastructure for scalable adaptive finite element methods and its application hp least squares C^∞ colocation. PhD dissertation, The University of Texas at Austin, Austin, TX, USA
26. Garcia O, Fancello EA, de Barcellos CS, Duarte CA (2000) *hp*-Clouds in Mindlin's thick plate model. Int J Numer Methods Eng 47:1381–1400
27. Gingold RA, Monaghan JJ (1982) Kernel estimates as a basis for general particle methods in hydrodynamics. J Comput Phys 46:429–453
28. Griebel M, Schweitzer MA (2000) A particle-partition of unity method for the solution of elliptic, parabolic and hyperbolic pdes. SIAM J Sci Comput 22:853–890
29. Kirchhoff GR (1850) Uber das Gleichgewicht und die Bewegung Einer Elastichen Scheibe. J Reine Angew Math 40:51–88
30. Krysl P, Belytschko T (1996) Analysis of thin plates by the element-free Galerkin method. Comput Mech 17:26–35
31. Krysl P, Belytschko T (1996) Analysis of thin shells by the element-free Galerkin method. Int J Solids Struct 33:3057–3080
32. Liu WK, Jun S, Zhang Y (1995) Reproducing kernel particle methods. Int J Numer Methods Eng 20:1081–1106
33. Lu H, Li S, Simkins DC Jr, Liu WK, Cao J (2004) Reproducing Kernel Element Method. Part III: Generalized enrichment and applications. Comput Methods Appl Mech Eng 193:989–1011
34. Melenk JM (1995) On generalized finite element methods. PhD Thesis. University of Maryland, College Park
35. Moës N, Dolbow J, Belytschko T (1999) Elastic crack growth in finite elements without remeshing. Int J Numer Methods Eng 46:131–150
36. Nicolazzi LC, Duarte CA, Fancello EA, de Barcellos CS (1997) *hp*-Clouds—a meshless method in boundary elements. Part II: implementation. Int J Boundary Element Methods Commun 8: 83–85
37. Nayroles B, Touzot G, Villon P (1992) Generalizing the finite element method: diffuse approximation and diffuse elements. Comput Mech 10:307–318
38. Oden JT, Duarte CA, Zienkiewicz OC (1998) A new cloud-based *hp* finite element method. Comput Methods Appl Mech Eng 153:117–126
39. Reddy JN (1997) Mechanics of laminated composite plates and shells, 2nd edn. CRC Press, USA
40. Rvachev VL, Sheiko TI (1995) R-functions in boundary value problems in mechanics. Appl Mech Rev 48(4):151–188
41. Shapiro V (1991) Theory of R-functions and applications: a primer. Technical report TR91-1219, Computer Science Department, Cornell University, Ithaca, NY
42. Shepard D (1968) A two-dimensional function for irregularly spaced data. In: ACM National Conference, pp 517–524
43. Simkins DC Jr, Li S, Lu H, Liu WK (2004) Reproducing kernel element method. Part IV: Globally compatible $C^n (n \geqq 1)$ triangular hierarchy. Comput Methods Appl Mech Eng 193:1013–1034
44. Stoker JJ (1942) Mathematical problems connected with the plate bending and buckling of elastic plates. Bull Am Math Soc 48: 247–261
45. Strouboulis T, Copps K, Babuska I (2001) The generalized finite element method. Comput Methods Appl Mech Eng 190: 4081–4193
46. Sukumar N, Moran B, Belytschko T (1998) The natural element method. Int J Numer Methods Eng 43:839–887
47. Whitney JM (1987) Structural analysis of laminated anisotropic plates. Technomic Publications Inc, Lancaster